SUPPLEMENTAL MATERIAL

Inclusion of cations in nucleic acids simulations

It is to be noted that, for several reasons, we mostly prefer to run simulations with minimal set of neutralizing Na^+ ions. This, considering the number of water molecules, results in salt concentration of ca. 0.2 M. We have several points to justify this choice.

1) The non-polarizable pair additive force field relies on a quite primitive approximation, representing the ions as simple van der Waals spheres with point charges +1 or +2. Thus, in fact, the force field is unlikely to fully capture for example the Na^+ vs. K^+ difference. One should not expect that matching exact ion concentrations as in the experiments is always desirable and meaningful since properties of the force-field ions are not those of real cations. More cations in the simulation could mean more possible problems due to force field bias.
2) The Na^+ parameters are the best tested, at least with the present solute and solvent force fields. As shown by us earlier, the current Na^+ parameters give the ion little oversized, i.e., somewhat in-between "real" Na^+ and K^+ (1).
3) The inaccuracy of inclusion of the Mg^{2+} ions is necessarily even much larger, due to neglect of large polarization and charge-transfer effects (2). This sharply limits accuracy of the simulation. The sampling by divalent cations is very poor, so the simulations cannot provide a proper distribution of divalent cations, in contrast to monovalents. The first shell water molecules of Mg^{2+} exchange on a microsecond scale, much above the simulation time scale. Improperly placed divalent cation can easily disturb the solute structure in a way that is not reparable on the simulation timescale (3).
4) It is worth to mention that inclusion of Cl^- anions into simulation could be quite risky, since anions are inherently polarizable species. Thus, their (pair additive) force field description is necessarily less accurate than for monovalent cations. In some unpublished simulations with KCl for G-DNA, we noticed formation of a KCl salt cluster in the box, hinting at evident imbalance of the KCl force field.
5) The simulations are too short to experience any unfolding due to imperfect ion conditions, in contrast to solution experiments. We have demonstrated this for ribosomal Kink-turns (4) which unfold in experiments unless high concentrations of divalents are present. Our unpublished simulations on 16S rRNA helix 44 show that its structure and flexibility are little affected even by excessive concentration of Mg^{2+}.
6) Several recent studies in addition indicate good performance of the simulations with minimal salt. Based on simulations of Kastenholz and Hunenberger (5), periodicity effects tend to be minimized in simulations with minimal, net-neutralizing salt (in contrast to zero or excess salt). Simulations by Varnai and Zakrzewska (6) have also demonstrated surprisingly good sampling of monovalent ions (in minimal salt) which is fully in agreement with the present paper and our preceding RNA simulation papers.

In summary, we suggest that performing the simulations in presence of minimal neutralizing Na^+ conditions is a wise option and the short time scale of the simulations prevents majority of artifacts that would result form this salt condition. Attempts to make the ion conditions more "physiological" may, in fact, cause more problems.

Electrostatics, FFT grid size, kappa values, switching function

The correct treatment of electrostatic interactions is provided by the PME method implemented in the Sander module of AMBER program package. Default values of input

PME parameters were used in our MD simulations because they represent the optimal settings appropriate for solvated systems. The size of the FFT charge grid in each dimension is set automatically using the periodic box dimensions. The FFT grid values are a product of powers of 2, 3 and 5 and they are leading to a grid spacing of ca. 1.0 Å. Kappa parameter (called Ewald coefficient in Sander) is not explicitly set (by default) and is determined by the direct sum tolerance (default value 10^{-5}) and the non-bonded cutoff limiting direct space sum (set to 9.0 Å). It results to the Ewald coefficient value of 0.30 $Å^{-1}$. No switching function for van der Waals interactions was used except a continuum model correction for energy and pressure applied to VDW interactions beyond those included in the direct sum.

Mg^{2+} is expelled from the active site in simulations of product and C75H^{+} protonated precursor ribozyme – detail description

Protonation of C75 would be required for its role as the acid in the catalysis. As described in detail earlier (7), protonated C75H^{+} moves towards its product location in Na^{+}-only precursor simulations and establishes a stable H-bonding network within the catalytic pocket. The same behavior is seen all along the new simulation with Mg^{2+} initially placed at the pocket (Table 1 in the main text). Actually, the Mg^{2+} cation escapes the active site 0.5 ns into the simulation PreC41+C75+Mg. It then makes direct contact to U23(O2P) and water-mediated contact to C24(O2P) outside the pocket ca. 9 Å away from the initial placement. The Mg^{2+} expulsion is consistent with the known competition between C75 protonation and Mg^{2+} binding at the active site (8).

No magnesium cation is observed at the cleavage site in wild-type and C75U product crystal structures. In product simulation ProC41+Mg with Mg^{2+} cation initially placed at the pocket (assuming outer shell binding), the cation is expelled from the pocket during the equilibration and remains again bound to U23 phosphate. The new location overlaps with a position of Mg^{2+} ion in the crystal structure of wild-type product, closest to the active site (Fig. 2A in the main text). The very swift expulsions of the ions indicate that the ion binding is destabilized substantially.

The cation binding associated with J4/2

Table S1 Inner-shell Na^{+}-binding occupancies (%) of individual atoms higher than 10% and number of exchanged cations (in parentheses) in binding sites *NA3* and *NA4*.

Site	Atom	Simulation				
		PreC41+	PreC41+C75+	PreC41+U75	ProC41+	ProC41+C75+
NA3	U20(O1P)	36(5)	26(2)	24(4)	24(4)	37(7)
	C21(O1P)	17(1)	35(1)	-	34(1)	23(3)
	C/U75(O2P)	22(2)	-	21(3)	84(3)	49(3)
Total		48	49	31	100	50
NA4	C32(O2P)	23(9)	33(7)	33(6)	23(9)	57(8)
	G31(O1P)	13(5)	14(3)	-	28(3)	13(4)
	A78(O1P)	-	22(4)	-	22(8)	35(8)
	A77(O2P)	11(3)	43(9)	-	-	14(5)
	A77(N7)	34(3)	38(2)	-	-	-
	A78(N7)	28(4)	12(2)	24(3)	80(3)	39(3)
Total		56	80	45	100	95

Table S2 Major groove Na^{2+} binding at GpG and ApG steps in representative product and precursor simulations: inner-shell occupancies (%) and number of exchanged cations (in parentheses).

Site	Atom	PreC41+A2	ProC41+
NA5	G1(N7)	44(4)	25(8)
	G1(O1P)	30(3)	-
	G2(N7)	15(2)	10(4)
	C75(N3)	16(4)	-
NA6	G5(N7)	42(5)	43(4)
	G6(N7)	11(4)	10(2)
NA7	A16(N7)	40(4)	12(4)
	G17(N7)	32(4)	11(3)
NA8	G28(N7)	31(4)	12(3)
	G29(N7)	13(3)	10(3)
NA9	G34(N7)	45(5)	30(4)
	G35(N7)	10(3)	19(5)
NA10	G39(O6)	22(6)	16(6)
	G40(O6)	40(7)	38(7)
	G40(N7)	30(7)	27(11)
NA11	G81(N7)	25(7)	17(6)
	G82(N7)	13(5)	10(4)

Details about major groove Na^+ binding

For double helical segments, the simulations revealed well-determined cation-binding sites with moderate occupancies at each GpG step, i.e., G1pG2, G5pG6, G28pG29, G34pG35, G70pG71 and G81pG82 (Table S2). Na^+ cation binding is alternating between N7 of two neighboring guanines and occupancy of the 5'-G is always higher (Table S2). Typical inner-shell cation binding times for canonical GpG-steps are 0.2–2.0 ns. Such major groove binding of cations is typical for A-RNA (9).

Na^+ binding to the G28pG29 step is sensitive to the arrangement of adjacent G25/U20 base pair (see above) and is reduced in product simulations. While G1pG2 step shows moderate cation binding site in product simulations, it is enhanced by G1 phosphate, which is positioned close to G1(N7) atom in precursor. The cations mostly form N7-O2P bridge in simulations and reveal enhanced binding times 0.7-4.0 ns. Further, long residency Na^+ binding in the major groove was revealed at G39pG40 step between canonical G39=C21 and the W.C./H. G40/G74 base pairs, as well as at the A16pG17 step, where P2 stacks on P3 with high twist (40°) and reduced rise (2.85 Å). The non-canonical G39pG40 step reveals longer binding times than the canonical GpG steps (up to 4.0 ns). The interaction of Na^+ cations with G(O6) atoms in major groove of canonical helixes was less pronounced as compared to G(N7) atoms and was the most significant at GpC steps in agreement with previous studies (9). *NA5, NA6* and *NA11* binding sites locate close to positions of three Mg^{2+} in wild type product crystal.

Product simulations with nine Mg^{2+}

We have carried out several simulations with excess of Mg^{2+}.

The crystal structure of the self-cleaved form of the ribozyme contains nine RNA-bound magnesium ions (10). It was previously reported that several of these ions are located within 5Å of regions of negative electrostatic potential (11). However, there is no direct correspondence between major ESP minima and positions of Mg^{2+} (see above, Fig. 2A).

Further, locations of only three magnesium ions are within 5Å from Na^+ binding sites (NA5, NA6 and weak site NA11) observed in MD simulations (Fig. 2, Table S2). We have thus carried out the ProMg simulation assuming this initial Mg^{2+} distribution. Most (7 of 9) Mg^{2+} ions show only small adjustments in the 15 ns simulation, which nevertheless is enough to place one Mg^{2+} cation to NA3 binding site. To obtain an additional insight into the Mg^{2+} binding to product, we conducted simulation ProC41+9Mg with 9 Mg^{2+} cations shifted away from the solute to the bulk (Table 1). After 10 ns of simulation, 4 Mg^{2+} cations were localized in positions exactly corresponding to cation binding sites NA11, NA10, MG2 and NA4 (only NA11 is close to Mg^{2+} position in product crystal, see above) and stayed bound till the end of 15 ns simulation. None of the remaining cations located within 5Å from any product Mg^{2+} crystal position. Obviously, the simulation time scale was very limited for divalents and thus Mg^{2+} binding was not converged in our simulations. Nevertheless, assessing all the data including Na^+ simulations that provide sufficient sampling we suggest that the simulations are not consistent with the overall positioning of Mg^{2+} cations in the wild-type product crystal structure. In contrast, dynamics of cations seen in simulations is entirely consistent with Mg^{2+} binding in the precursor and C75U product crystal structures.

REFERENCES

1. Spackova, N., I. Berger, and J. Sponer. 1999. Nanosecond molecular dynamics simulations of parallel and antiparallel guanine quadruplex DNA molecules. J. Am. Chem. Soc. 121: 5519-5534.
2. Gresh, N., J.E. Sponer, N. Spackova, J. Leszczynski, and J. Sponer. 2003. Theoretical study of binding of hydrated Zn(II) and Mg(II) cations to 5 '-guanosine monophosphate. Toward polarizable molecular mechanics for DNA and RNA. J. Phys. Chem. B 107: 8669-8681.
3. Reblova, K., N. Spackova, J. Koca, N.B. Leontis, and J. Sponer. 2004. Long-residency hydration, cation binding, and dynamics of loop E/helix IV rRNA-L25 protein complex. Biophys. J. 87: 3397-3412.
4. Razga, F., J. Koca, J. Sponer, and N.B. Leontis. 2005. Hinge-like motions in RNA kink-turns: The role of the second A-minor motif and nominally unpaired bases. Biophys. J. 88: 3466-3485.
5. Kastenholz, M.A. and P.H. Hunenberger. 2004. Influence of artificial periodicity and ionic strength in molecular dynamics simulations of charged biomolecules employing lattice-sum methods. J. Phys. Chem. B 108: 774-788.
6. Varnai, P. and K. Zakrzewska. 2004. DNA and its counterions: a molecular dynamics study. Nucleic Acids Res. 32: 4269-4280.
7. Krasovska, M.V., J. Sefcikova, N. Spackova, J. Sponer, and N.G. Walter. 2005. Structural Dynamics of Precursor and Product of the RNA Enzyme from the Hepatitis Delta Virus as Revealed by Molecular Dynamics Simulations. J. Mol. Biol. 351: 731-748.
8. Nakano, S., D.M. Chadalavada, and P.C. Bevilacqua. 2000. General acid-base catalysis in the mechanism of a hepatitis delta virus ribozyme. Science. 287: 1493-1497.
9. Auffinger, P. and E. Westhof. 2000. Water and ion binding around RNA and DNA (C,G) oligomers. J. Mol. Biol. 300: 1113-1131.
10. Ferre-D'Amare, A.R., K. Zhou, and J.A. Doudna. 1998. Crystal structure of a hepatitis delta virus ribozyme. Nature. 395: 567-574.

11. Nakano, S., D.J. Proctor, and P.C. Bevilacqua. 2001. Mechanistic characterization of the HDV genomic ribozyme: assessing the catalytic and structural contributions of divalent metal ions within a multichannel reaction mechanism. Biochemistry. 40: 12022-12038.

SUPPLEMENTAL MATERIAL - Figures

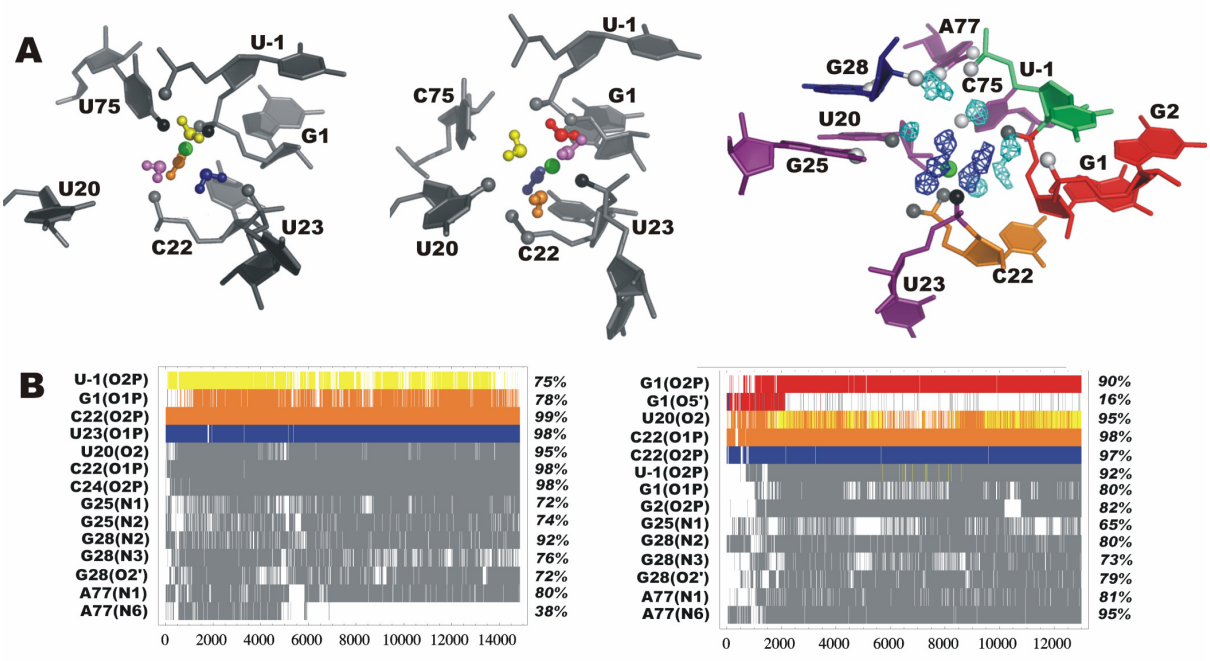

Fig. S1.
(A) First hydration shell of Mg^{2+} bound at the catalytic pocket in simulations PreC41+U75A2Mg (left) and PreC41+A2Mg before the G1(O5')…Mg^{2+} water bridge was broken (middle). Right - first and second hydration shells of the catalytic Mg^{2+} in the simulation PreC41+A2Mg (after the G1(O5')…Mg^{2+} water bridge was lost). The residues are color-coded as shown at Fig. 1, Mg^{2+} is represented by green ball; dark blue and cyan mesh – first and second hydration shell of Mg^{2+}. Functional groups of the catalytic pocket directly bound to Mg^{2+} are black balls, those bound to the first hydration shell waters are gray balls and those bound to the second hydration shell waters are white balls. (B) Dynamics of water bridges between Mg^{2+} and the ribozyme atoms; the first shell water molecules are color coded as on the stick models (A, left and middle) while the second shell water molecules are gray. The criterion to include water molecules into the first and second hydration shell was maximal distance from Mg^{2+} 3.0 and 4.5 Å, respectively; the H-bonding criterion was distance between heavy atoms (water and solute) ≤3.4 Å. Both criteria must be satisfied to identify the bridge.

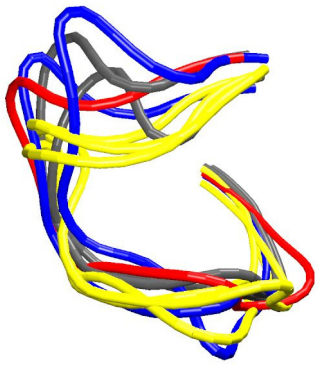

Fig. S2.
The overlay of L3 backbone based on the global structure superposition. The U75 precursor crystal structure (red) and simulated structures (averaged over 10-13ns interval; color coded according to the type of U20/G25 base pair): Bifurcated *cis*-W.C./W.C. in simulations with Mg^{2+} bound in the L3 pocket (grey), *cis*-W.C./W.C. base pair in absence of Mg^{2+} (blue) and *trans*-W.C/H. base pair in absence of Mg^{2+}(yellow).

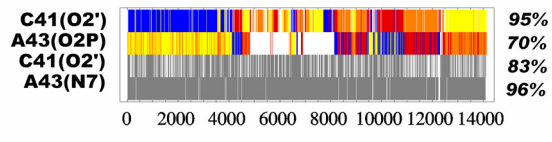

Fig. S3.
Dynamics of the water bridges between Mg^{2+} bound at the MG2 binding site and ribozyme in simulation PreC41+A2Mg; the individual water molecules in the first hydration shell are shown by different colors and the second shell water molecules are gray. The binding criteria are the same as on Fig. S1.

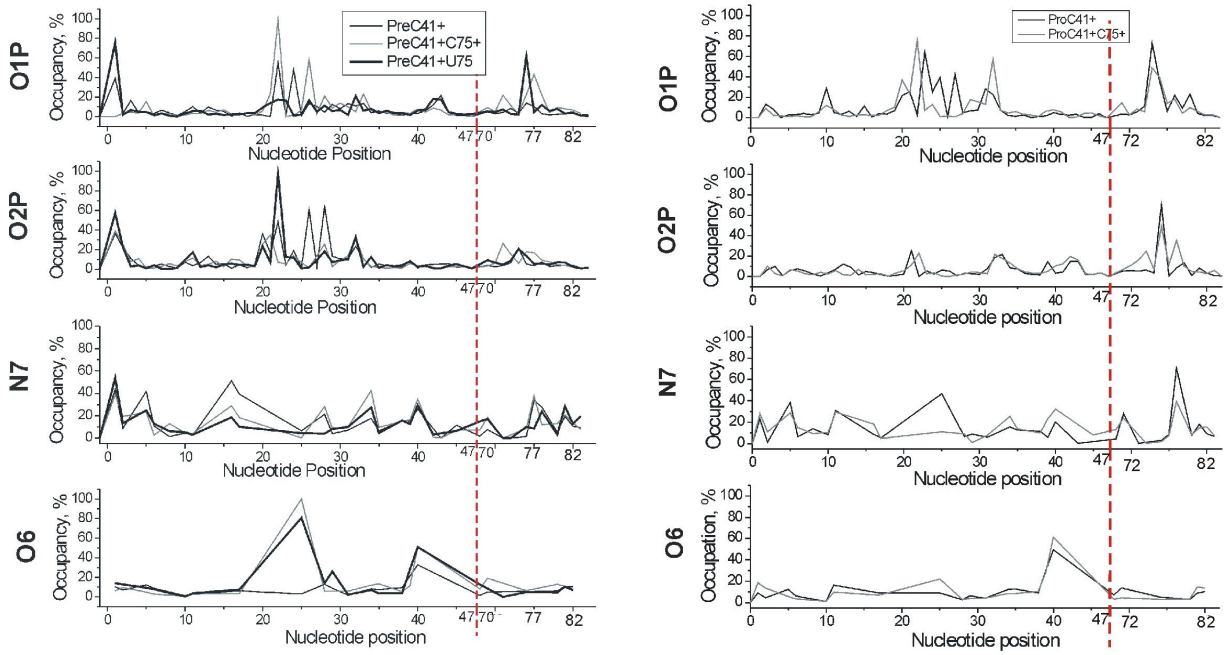

Fig. S4.
Inner shell binding of Na^+: the total occupancies of the electronegative atoms in simulations of product (right) and precursor (left) HDV ribozyme. The red line marks the P4 truncation, which causes the gap in base numbering.

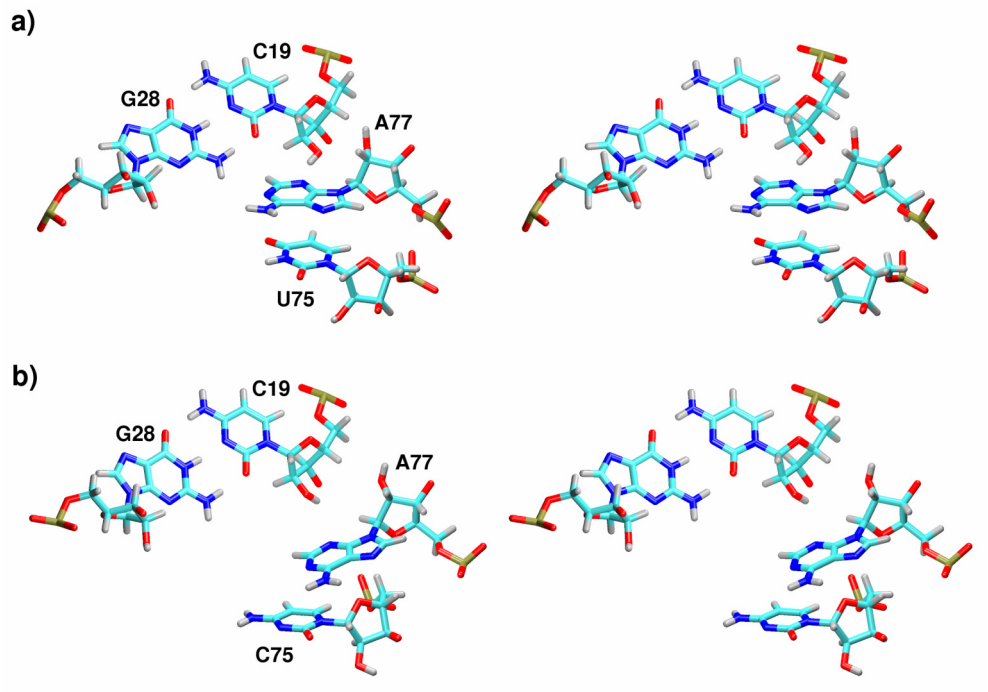

Fig. S5.
Stereo view of different geometries observed in the area of the A-minor type II motif and the residue at position 75. a) The closed A-minor interaction and maximal base-base overlap of U75 and A77 observed in simulation PreC41+U75. b) The open A-minor geometry and the mutual shift of C75/A77 bases leading to sugar-base stacking observed in simulation PreC41+Mg.

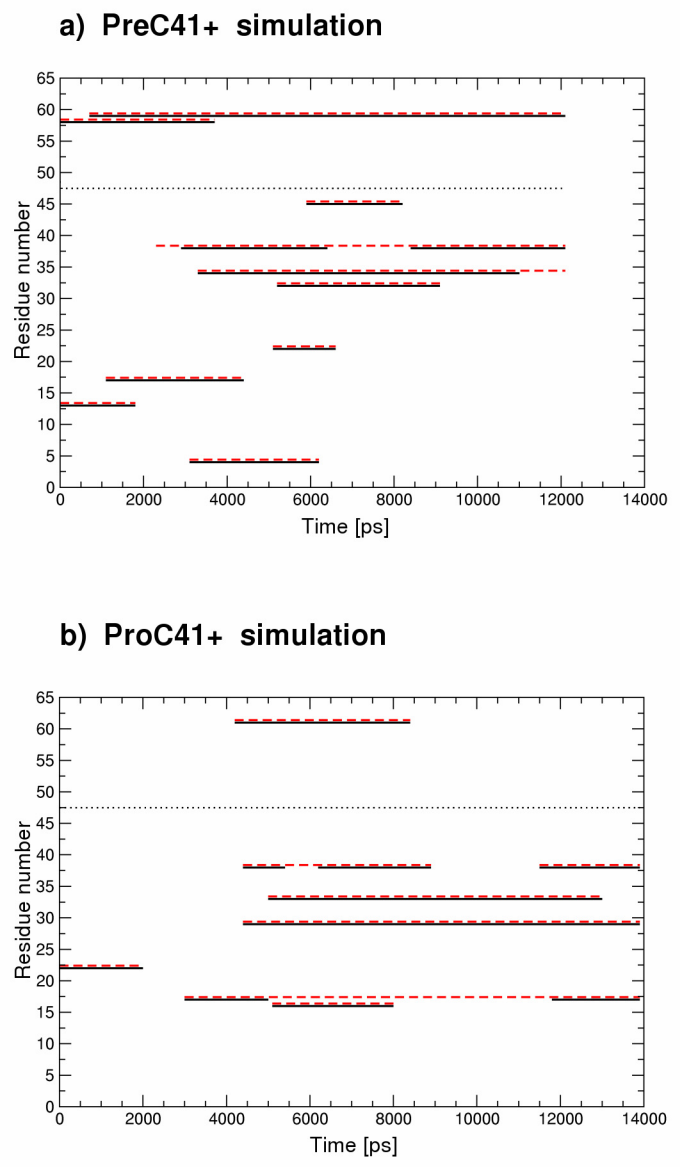

Fig. S6.
α/γ switches observed in the 12 ns precursor simulation PreC41+ (a) and in the 14 nsproduct simulation ProC41+ (b). The black line represents α values of ~155°, the red dashed line represents γ values of ~180°. Residues 70-84 (above the dotted line) are re-numbered as 48-62 for the purpose of this Figure. The Figure shows only nucleotides involved in Watson-Crick segments of the HDV ribozyme. It is visible that the RNA α/γ are reversible (in contrast to B-DNA simulations), in agreement with our multiple 25 ns simulations of sarcin-ricin loop and 30-40 ns of 16S rRNA helix 44 and canonical RNA.